

# Neutrino-Deuteron Reactions at Solar Neutrino Energies in Pionless Effective Field Theory with Dibaryon Fields

Shung-Ichi Ando,<sup>1,\*</sup> Young-Ho Song,<sup>2</sup> and Chang Ho Hyun<sup>3</sup>

<sup>1</sup>*School of Mechanical and ICT Convergence Engineering,  
Sunmoon University, Asan, Chungnam 31460, Korea*

<sup>2</sup>*Rare Isotope Science Project, Institute for Basic Science, Daejeon 34047, Korea<sup>†</sup>*

<sup>3</sup>*Department of Physics Education, Daegu University, Gyeongsan 38453, Korea<sup>‡</sup>*

(Dated: May 17, 2022)

## Abstract

We study breakup of the deuteron induced by neutrinos in the neutral  $\nu d \rightarrow \nu np$ ,  $\bar{\nu} d \rightarrow \bar{\nu} np$  and the charged  $\bar{\nu} d \rightarrow e^+ nn$ ,  $\nu d \rightarrow e^- pp$  processes. Pionless effective field theory with dibaryon fields is used to calculate the total cross sections for the neutrino energies  $E_\nu$  from threshold to 20 MeV. Amplitudes are expanded up to next-to-leading order, and the partial wave is truncated at P-waves. Coulomb interaction between two protons is included non-perturbatively in the reaction amplitudes, and an analytic expression of the amplitudes is obtained. Contribution of the next-to-leading order to the total cross section is in the range of 5.2~9.9% in magnitude, and that of P-wave is 2.4~2.8% at  $E_\nu = 20$  MeV. Uncertainty arising from an axial isovector low-energy constant is estimated at the order of 1%.

---

\*Electronic address: sando@sunmoon.ac.kr

†Electronic address: yhsong@ibs.re.kr

‡Electronic address: hch@daegu.ac.kr

## I. INTRODUCTION

Since first postulated by W. Pauli, neutrinos have played key roles in understanding the nature of weak interactions, and testing the standard model [1]. These fundamental questions can be answered directly or indirectly by measuring the cross sections of neutrinos. Measurements have been conducted with neutrinos from man-made sources and various events in the Universe. Corresponding energy scale is indeed wide, ranging from eV to EeV<sup>1</sup>. Neutrinos in the energy range from 1 to 20 MeV are particularly important in probing the solar process and flavor oscillation of neutrinos. The solar neutrinos on the deuteron target are measured at SNO, and the neutrino flavor mixing parameters are deduced by using the  $\nu d$  cross sections estimated by theory [2–5]. Meanwhile, direct measurements on deuteron target in the solar neutrino range have been carried out in the reactor experiments. They reported cross sections for the charged-current process  $\bar{\nu}_e d \rightarrow e^+ nn$ , and the neutral-current process  $\bar{\nu}_e d \rightarrow \bar{\nu}_e np$  [6–9]. Comparison of experiments with theory exhibits qualitative agreement [10].

Early theoretical estimates of the neutrino reactions on the deuteron are reported in the 1960s [11, 12] while modern ones are improved by using accurate phenomenological nucleon-nucleon ( $NN$ ) potentials and including meson exchange currents [13–15]. Modern theories of  $NN$  interactions can reproduce the  $NN$  scattering phase shift data below the pion production threshold with errors less than 1%. These high-precision theories provide a unique opportunity in which we can probe the interactions of neutrino and deuteron with uncertainties due to strong interactions under control. In the publications during the last decade, we have been applying the pionless effective field theory with dibaryon fields (dEFT in short) [16, 17] to the low-energy two-nucleon systems and phenomena such as electromagnetic (EM) form factors of the deuteron [18], synthesis of the deuteron at big bang energies [19], proton-proton scattering [20], their fusion [21], neutron-proton scattering [22], spin-dependent polarization [23–25], and hadronic parity violation in the radiative neutron-proton fusion or the dissociation of the deuteron [26–30]. We could verify that i) calculational complexity and difficulty are significantly reduced in dEFT compared to the calculations in phenomenological potential models or other EFTs, ii) convergence of the

---

<sup>1</sup> EeV is an initialism of exa-electron volt,  $10^{18}$  eV.

expansion is fast so only up to next-to-next-to-leading order (NNLO), results agree to high-quality calculation of phenomenological models, and iii) agreement to experiment and other theories is achieved with difference less than 1% at low energies.

Inspired by the successful applications to the strong and EM interactions and related phenomena, we attempt to apply the model to a semi-leptonic weak interaction problem, breakup of the deuteron by neutrinos at low energies. Solution of the problem plays an important role in understanding the flavor oscillation of neutrinos from the sun, and testing the validity of the standard model. In addition, it has been discussed that the process can give non-negligible effect to the supernova neutrino emission mechanism [31]. The problem has been explored in diverse frameworks such as conventional approach of two-nucleon potential plus meson exchange currents [14], hybrid EFT [32], pionless EFT [33], and a recent work with chiral perturbation theory [34]. The results in various theoretical works agree to high accuracy.

In this work we focus on two issues: i) estimate the uncertainty of the prediction, ii) investigate the convergence and accuracy of the expansion in dEFT formalism. We calculate the total cross sections of the neutral-current processes

$$\nu_l d \rightarrow \nu_l np, \quad \bar{\nu}_l d \rightarrow \bar{\nu}_l np, \quad (1)$$

where  $l$  denotes the lepton flavor  $e$ ,  $\mu$  and  $\tau$ , and the charged-current processes

$$\nu_e d \rightarrow e^- pp, \quad \bar{\nu}_e d \rightarrow e^+ nn, \quad (2)$$

with neutrino energy from threshold to 20 MeV. We consider the expansion up to next-to-leading order (NLO) and assume P-wave approximation for the partial-wave expansion in the final state of the nucleon. In addition, we include the Coulomb interaction between two protons non-perturbatively and obtain an analytic expression for the reaction amplitudes for the  $\nu_e d \rightarrow e^- pp$  process. Results are compared to the results of most updated calculations with modern potential models and EFTs.

Section II summarizes the basic equations, and analytic forms of transition amplitudes and the cross sections. Numerical results are presented in Section III, and the conclusions are drawn in Section IV. In Appendix A, a derivation of an analytic expression of the reaction amplitudes for the  $\nu_e d \rightarrow e^- pp$  process is presented, and in Appendix B, the spin summation relations and an expression of the squared amplitudes are displayed.

## II. ANALYTIC EXPRESSION FOR THE REACTION AMPLITUDES

### A. Weak process and dibaryon EFT

The reaction amplitudes can be calculated from the effective Hamiltonian of the current-current interaction [1]

$$H = \frac{G'_F}{\sqrt{2}} \int d^3x [V_{ud} J_\mu^{(CC)}(\vec{x}) l^{(CC)\mu}(\vec{x}) + J_\mu^{(NC)} l^{(NC)\mu}(\vec{x})], \quad (3)$$

where  $G'_F = 1.1803 \times 10^{-5} \text{ GeV}^{-2}$  is the weak coupling constant, and  $V_{ud} = 0.9746$  is a Kobayashi-Maskawa matrix element. Note that  $G'_F$  includes the inner radiative corrections:  $G'^2_F = G^2_F(1 + \Delta^V_R)$ , where  $G_F = 1.1166 \times 10^{-5} \text{ GeV}^{-2}$  is the Fermi constant and  $\Delta^V_R$  is the inner radiative correction [35, 36]. The CC- and NC-lepton currents  $l_\mu^{(CC)}$  and  $l_\mu^{(NC)}$  are well known, and the CC- and NC-hadron currents  $J_\mu^{(CC)}$  and  $J_\mu^{(NC)}$  are written as

$$J_\mu^{(CC)} = V_\mu^\pm(\vec{x}) - A_\mu^\pm(\vec{x}), \quad (4)$$

$$J_\mu^{(NC)} = (1 - \sin^2 \theta_W) V_\mu^0(\vec{x}) - A_\mu^0(\vec{x}) - 2 \sin^2 \theta_W V_\mu^S(\vec{x}), \quad (5)$$

where  $V_\mu$  and  $A_\mu$  represent the vector and axial current, respectively. The superscripts  $\pm$  and 0 are the isospin indices of the isovector current and  $S$  denotes the isoscalar current.  $\theta_W$  is the Weinberg angle with the numerical value  $\sin^2 \theta_W = 0.2312$ .

The CC- and NC-hadronic currents  $J_\mu^{(CC)}$  and  $J_\nu^{(NC)}$  are calculated from the Lagrangians for the  $\nu d$  scattering relevant up to NLO [18, 21, 38]

$$\mathcal{L} = \mathcal{L}_0 + \mathcal{L}_1 + \mathcal{L}_t + \mathcal{L}_s + \mathcal{L}_{\text{int}}, \quad (6)$$

where  $\mathcal{L}_0$  and  $\mathcal{L}_1$  are leading order (LO) and NLO one-nucleon Lagrangians,  $\mathcal{L}_s$  and  $\mathcal{L}_t$  are the Lagrangians for dibaryon-dibaryon and dibaryon-nucleon couplings in the  $^1S_0$  and  $^3S_1$  states, respectively, and  $\mathcal{L}_{\text{int}}$  denotes the EM and weak interactions of nucleons and dibaryons through external vector and axial-vector fields.

The Lagrangian for the one-nucleon sector is given as [36]

$$\mathcal{L}_0 = N^\dagger [iv \cdot \tilde{D} + 2g_A S \cdot a] N, \quad (7)$$

$$\begin{aligned} \mathcal{L}_1 = \frac{1}{2m_N} N^\dagger & \left[ (v \cdot \tilde{D})^2 - \tilde{D}^2 - 2ig_A \{v \cdot a, S \cdot \tilde{D}\} \right. \\ & \left. - 2i(1 + \kappa_V)[S^\mu, S^\nu] f_{\mu\nu}^+ - 2i(1 + \kappa_S)[S^\mu, S^\nu] v_{S\mu\nu} \right] N, \end{aligned} \quad (8)$$

with

$$\tilde{D}^\mu = \partial^\mu - i\frac{1}{2}\tau_a \cdot v_a^\mu - i\frac{1}{2}v_S^\mu, \quad a^\mu = \frac{1}{2}\tau_a \cdot a_a^\mu, \quad (9)$$

$$f_{\mu\nu}^+ = \partial_\mu \left( \frac{1}{2}\tau_a \cdot v_{a\nu} \right) - \partial_\nu \left( \frac{1}{2}\tau_a \cdot v_{a\mu} \right), \quad v_S^{\mu\nu} = \frac{1}{2}(\partial^\mu v_S^\nu - \partial^\nu v_S^\mu), \quad (10)$$

where  $g_A$  is the axial vector coupling constant  $g_A = 1.267$ ,  $m_N$  is the mean nucleon mass  $m_N = (m_p + m_n)/2$ ,  $\kappa_V$  and  $\kappa_S$  are the isovector and isoscalar anomalous magnetic moment of the nucleon  $\kappa_V = 3.70589$  and  $\kappa_S = -0.12019$ , respectively.  $v^\mu$  is the velocity vector satisfying  $v^2 = 1$ . Assuming non-relativistic limit, we have  $v^\mu = (1, \vec{0})$ , which subsequently determines the spin operator  $2S^\mu = (0, \vec{\sigma})$ .  $v_S^\mu$ ,  $v_a^\mu$  and  $a_a^\mu$  are the external isoscalar, isovector and axial isovector fields, respectively, and  $\tau_a$  and  $\sigma_i$  are the Pauli matrices for the iso-spin and spin, respectively.

The Lagrangian for the two-nucleon sector is given as

$$\mathcal{L}_s = \sigma s_a^\dagger \left[ iv \cdot D + \frac{1}{4m_N} [(v \cdot D)^2 - D^2] + \Delta_s \right] s_a - y_s \left[ s_a^\dagger (N^T P_a^{(1S_0)} N) + \text{h.c.} \right], \quad (11)$$

$$\mathcal{L}_t = \sigma t_i^\dagger \left[ iv \cdot D + \frac{1}{4m_N} [(v \cdot D)^2 - D^2] + \Delta_s \right] t_i - y_t \left[ t_i^\dagger (N^T P_i^{(3S_1)} N) + \text{h.c.} \right], \quad (12)$$

$$\begin{aligned} \mathcal{L}_{\text{int}} &= \frac{L_{1A}}{m_N \sqrt{\rho_d r_0}} [a_a^i t^{i\dagger} s_a + \text{h.c.}] + \frac{L_1}{m_N \sqrt{\rho_d r_0}} [B_a^i t^{i\dagger} s_a + \text{h.c.}] \\ &+ \frac{L_{2A}}{m_N \sqrt{\rho_d r_0}} [i(\vec{D}a_a^0) \cdot \vec{t} s_a + \text{h.c.}], \end{aligned} \quad (13)$$

where  $D_\mu$  is the covariant derivative for the dibaryon fields,  $D_\mu = \partial_\mu - iC\mathcal{V}_\mu^{ext}$ ;  $\mathcal{V}^{ext}$  is the external vector field and  $C$  is the charge operator of the dibaryon fields where  $C = 0, 1$ , and  $2$  for the  $nn$ ,  $np$ , and  $pp$  channels, respectively. (See footnote 6 in Ref. [18] as well.) In addition,  $\vec{B} = \nabla \times \vec{v}_a$ , and  $\sigma$  is the sign factor (+1 or -1), which is fixed so as to reproduce the amplitude in terms of the effective range expansion parameters.  $\Delta_s$  and  $\Delta_t$  are defined as  $\Delta_{s,t} \equiv m_{s,t} - 2m_N$  where  $m_s$  and  $m_t$  are the mass of dibaryon fields in the  $^1S_0$  and  $^3S_1$  states, respectively.  $\rho_d$  and  $r_0$  are the effective ranges in the  $^1S_0$  and  $^3S_1$  states, and the projection operators for each state are defined as

$$P_a^{(1S_0)} = \frac{1}{\sqrt{8}}\sigma_2\tau_2\tau_a, \quad P_i^{(3S_1)} = \frac{1}{\sqrt{8}}\sigma_2\sigma_i\tau_2. \quad (14)$$

Moreover,  $y_s$  and  $y_t$  are determined from the effective range parameters, and we obtain

$$y_s^2 = -\frac{8\pi\sigma}{m_N^2 r_0}, \quad y_t^2 = -\frac{8\pi\sigma}{m_N^2 \rho_d}. \quad (15)$$

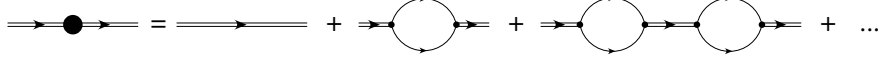


FIG. 1: Feynman diagrams for dressed dibaryon propagator for  $np$  and  $nn$  channels. A single curve denotes a propagation of nucleon while a double line with and without a filled circle does a propagation of a dressed and bare dibaryon, respectively.

Determination of  $L_{1A}$ ,  $L_1$  and  $L_{2A}$  will be discussed in section III.

Total cross section is calculated with the non-relativistic formula [32]

$$\sigma_{\nu d}(E_\nu) = \frac{1}{(2\pi)^3} \int dp \int dy \frac{p^2 k'^2}{2E_\nu E'} \frac{F(Z, E')}{k'/E' + (k' - E_\nu y)/(2m_N)} \frac{1}{2S_d + 1} \sum_{\text{spin}} |A_{(qq,np)}|^2, \quad (16)$$

with the condition for the energy-momentum conservation up to  $1/m_N$  order,

$$m_d + E_\nu - E' - 2m_N - \frac{1}{m_N} \left[ p^2 + \frac{1}{4} (E_\nu^2 + k'^2 - E_\nu k' y) \right] = 0, \quad (17)$$

where  $m_d$  is the mass of the deuteron,  $E_\nu$  ( $E'$ ) is the energy of the neutrino (lepton) in the initial (final) state,  $p$  is the magnitude of the relative three-momentum between the two nucleons in the final state,  $k'$  is that of the outgoing lepton, and  $y$  is the cosine of the angle between the incoming and the outgoing leptons ( $y = \hat{k} \cdot \hat{k}'$ ).  $F(Z, E')$  is the Fermi function taking into the Coulomb interactions between the electron and the nucleon in the final state; its explicit form can be found in Ref. [37]. Here,  $S_d$  is the total spin of the deuteron,  $S_d = 1$ . We note that the expression of the total cross section in Eq. (16) is different from that in our previous study [32] by a factor of  $1/(4E'E_\nu)$  because of different normalizations for the lepton fields. In addition, the fourth term,  $2m_N$ , in the left-hand side of Eq. (17) depends on the final two nucleon states:  $2m_N = 2m_n, 2m_p, m_n + m_p$  for the  $nn, pp, np$  states, where  $m_n$  and  $m_p$  are the masses of neutron and proton.  $A_{(nn,np)}$  are the transition amplitudes for the final  $nn$  and  $np$  channels which are calculated from the Feynman diagrams shown in Figs. 1 and 2, and  $A_{(pp)}$  is that for the final  $pp$  channels from those in Figs. 3 and 4. Diagrams (a, b, c) are the LO contributions, and (d, e, f) give the NLO contributions in Figs. 2 and 4.

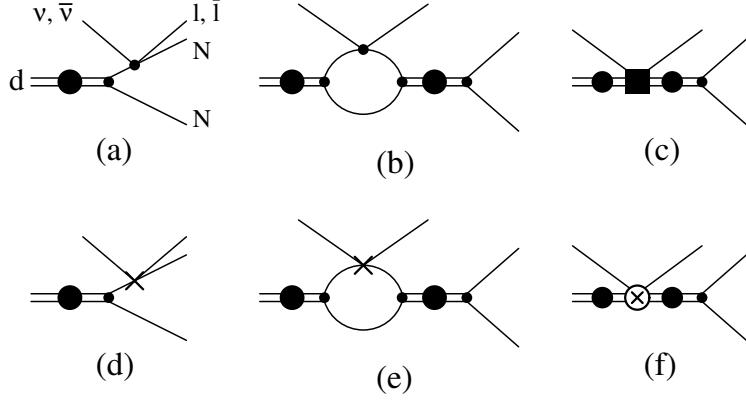


FIG. 2: Feynman diagrams for the  $\nu d \rightarrow l NN$  and  $\bar{\nu} d \rightarrow \bar{l} NN$  reactions without the Coulomb interaction between two nucleons at LO (a)–(c) and NLO (d)–(f). Vertices with a dot (a cross) interacting with a lepton current are those at LO (NLO) for single nucleon sector, and those with a filled box (a crossed circle) are vertices at LO (NLO) for double nucleon sector. See the caption in FIG. 1 as well.

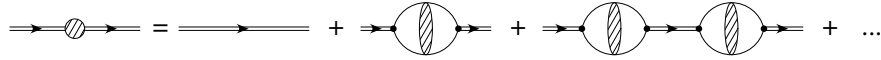


FIG. 3: Feynman diagrams for dressed dibaryon propagator for  $pp$  channel. Slashed blobs represent the non-perturbative Coulomb interaction between two protons, which include no interaction diagram and all possible diagrams exchanging a potential photon up to infinite order. See the caption in FIG. 1 as well.

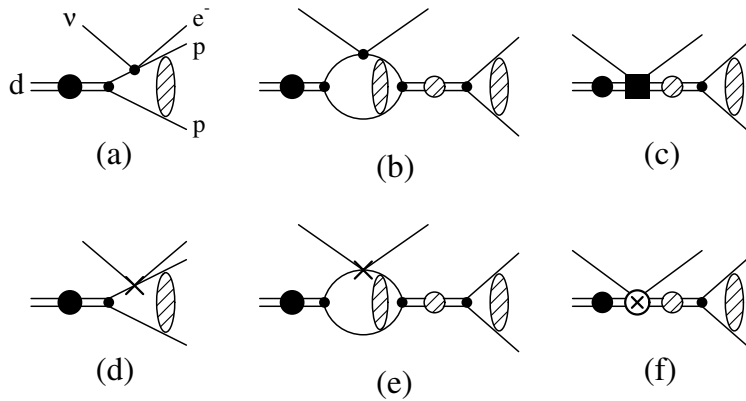


FIG. 4: Feynman diagrams for the  $\nu d \rightarrow e^- pp$  reaction at LO (a)–(c) and NLO (d)–(f). See the captions in FIGs. 1, 2, and 3 as well.

## B. Reaction amplitudes

We write the amplitudes of charged current as

$$A_{qq} = (-1)^{(1+\tau_q)/2} G'_F V_{ud} \left[ -\mathcal{A}_A^{1S0} + \tilde{\mathcal{A}}_V^{1S0} - \tilde{\mathcal{A}}_A^{1S0} + \sum_{J=0}^2 (\mathcal{A}_V^{3PJ} - \mathcal{A}_A^{3PJ}) \right], \quad (18)$$

where  $q$  denotes neutron ( $n$ ) or proton ( $p$ ), and  $\tau_{n(p)} = -1(1)$ . Leading order amplitudes are contributed from diagrams (a, b, c) in Figs. 2 and 4, and they are represented in terms of the untilded amplitudes  $\mathcal{A}$ . Tilded letters  $\tilde{\mathcal{A}}$  represent the amplitudes at NLO, and they are from diagrams (d, e, f) in Figs. 2 and 4. The superscripts and subscripts on the amplitudes denote the partial waves and spin states ( $^1S_0$ ,  $^3S_1$ , and  $^3P_J$  states) for the final two nucleons and isovector vector ( $V$ ) and axial-vector ( $A$ ) nuclear currents, respectively.

Neutral-current amplitudes are written as

$$A_{np} = \frac{G'_F}{\sqrt{2}} \left\{ (1 - 2 \sin^2 \theta_W) \left[ \tilde{\mathcal{A}}_V^{1S0} + \sum_{J=0}^2 \mathcal{A}_V^{3PJ} \right] - \left( \mathcal{A}_A^{1S0} + \tilde{\mathcal{A}}_A^{1S0} + \sum_{J=0}^2 \mathcal{A}_A^{3PJ} \right) - 2 \sin^2 \theta_W \left[ \mathcal{A}_{VS}^{3S1} + \tilde{\mathcal{A}}_{VS}^{3S1} \right] \right\}, \quad (19)$$

where the subscript ( $VS$ ) denotes the isoscalar vector part of the nuclear current. Because the partial waves are orthogonal, we can write the squared amplitudes as

$$|A_{qq}|^2 = G'^2_F V_{ud}^2 \left[ \left| -\mathcal{A}_A^{1S0} + \tilde{\mathcal{A}}_V^{1S0} - \tilde{\mathcal{A}}_A^{1S0} \right|^2 + \sum_{J=0}^2 \left| \mathcal{A}_V^{3PJ} - \mathcal{A}_A^{3PJ} \right|^2 \right], \quad (20)$$

$$|A_{np}|^2 = \frac{G'^2_F}{2} \left\{ \left| \mathcal{A}_A^{1S0} + \tilde{\mathcal{A}}_A^{1S0} - (1 - 2 \sin^2 \theta_W) \tilde{\mathcal{A}}_V^{1S0} \right|^2 + \left| 2 \sin^2 \theta_W (\mathcal{A}_{VS}^{3S1} + \tilde{\mathcal{A}}_{VS}^{3S1}) \right|^2 + \sum_{J=0}^2 \left| \mathcal{A}_A^{3PJ} - (1 - 2 \sin^2 \theta_W) \mathcal{A}_V^{3PJ} \right|^2 \right\}. \quad (21)$$

Amplitudes for S-wave states can be written as

$$\mathcal{A}_A^{1S0} = \vec{\epsilon}_{(l)} \cdot \vec{\epsilon}_{(d)} X_A^{1S0}, \quad (22)$$

$$\tilde{\mathcal{A}}_A^{1S0} = v \cdot \epsilon_{(l)} \hat{q} \cdot \vec{\epsilon}_{(d)} \tilde{X}_A^{1S0}, \quad (23)$$

$$\tilde{\mathcal{A}}_V^{1S0} = i \hat{q} \cdot (\vec{\epsilon}_{(d)} \times \vec{\epsilon}_{(l)}) \tilde{X}_V^{1S0}, \quad (24)$$

$$\mathcal{A}_{VS}^{3S1} = v \cdot \epsilon_{(l)} \vec{\epsilon}^* \cdot \vec{\epsilon}_{(d)} X_{VS}^{3S1}, \quad (25)$$

$$\tilde{\mathcal{A}}_{VS}^{3S1} = \hat{q} \cdot \vec{\epsilon}_{(l)} \vec{\epsilon}^* \cdot \vec{\epsilon}_{(d)} \tilde{X}_{VS}^{3S1}, \quad (26)$$



where  $\vec{\epsilon}_{(d)}$  and  $\vec{\epsilon}^*$  are spin polarization vectors of the incoming deuteron and the final two nucleon  ${}^3S_1$  state, respectively, and  $\epsilon_\mu^{(l)}$  are the lepton currents. In addition,  $\hat{q} = \vec{q}/|\vec{q}|$  where  $\vec{q}$  is the momentum transfer between the lepton current and the nuclear current;  $\vec{q} = \vec{k}' - \vec{k}$ .  $X$  and  $\tilde{X}$  denote the LO and NLO contributions, respectively, and are given by

$$X_A^{1S0} = 2g_A \sqrt{\frac{2\pi\gamma}{1-\gamma\rho_d}} \left\{ \Gamma_{4(1)}^{(NN)}(p, q) + \Gamma_{3(0)}^{(NN)}(p) D_s^{(NN)}(p) \left[ \Gamma_{3(1)}^{(NN)}(p, q) - \frac{1}{4}(r_0^{(NN)} + \rho_d) + \frac{l_{1A}}{2g_A m_N} \right] \right\}, \quad (27)$$

$$\tilde{X}_A^{1S0} = \frac{2g_A}{m_N} \sqrt{\frac{2\pi\gamma}{1-\gamma\rho_d}} \left\{ p \Gamma_{4(2)}^{(NN)}(p, q) + \Gamma_{3(0)}^{(NN)}(p) D_s^{(NN)}(p) q \left[ \Gamma_{3(2)}^{(NN)}(p, q) - \frac{1}{16}(r_0^{(NN)} + \rho_d) + \frac{l_{2A}}{4g_A} \right] \right\}, \quad (28)$$

$$\tilde{X}_V^{1S0} = -\frac{\mu_V q}{m_N} \sqrt{\frac{2\pi\gamma}{1-\gamma\rho_d}} \left\{ \Gamma_{4(1)}^{(NN)}(p, q) + \Gamma_{3(0)}^{(NN)}(p) D_s^{(NN)}(p) \left[ \Gamma_{3(1)}^{(NN)}(p, q) - \frac{1}{4}(r_0^{(NN)} + \rho_d) + \frac{l_1}{\mu_V} \right] \right\}, \quad (29)$$

$$X_{VS}^{3S1} = -2 \sqrt{\frac{2\pi\gamma}{1-\gamma\rho_d}} \left\{ \Gamma_{4(1)}^{(np)}(p, q) + \Gamma_{3(0)}^{(np)}(p) D_t^{(np)}(p) \left[ \Gamma_{3(1)}^{(np)}(p, q) - \frac{1}{2}\rho_d \right] \right\}, \quad (30)$$

$$\tilde{X}_{VS}^{3S1} = -\frac{2}{m_N} \sqrt{\frac{2\pi\gamma}{1-\gamma\rho_d}} \left\{ p \Gamma_{4(2)}^{(np)}(p, q) + \Gamma_{3(0)}^{(np)}(p) D_t^{(np)}(p) q \left[ \Gamma_{3(2)}^{(np)}(p, q) - \frac{1}{8}\rho_d \right] \right\}, \quad (31)$$

where  $\gamma$  is the deuteron binding momentum,  $\gamma = \sqrt{2m_N B}$ :  $B$  is the deuteron binding energy, and  $\mu_V = 1 + \kappa_V$ . The LECs  $l_{1A}$ ,  $l_{2A}$ , and  $l_1$  for the contact interactions are defined as

$$l_{1A} = L_{1A} + \frac{1}{2} m_N g_A (\rho_d + r_0^{(NN)}), \quad (32)$$

$$l_{2A} = L_{2A} + \frac{1}{4} g_A (\rho_d + r_0^{(NN)}), \quad (33)$$

$$l_1 = L_1 + \frac{1}{4} \mu_V (\rho_d + r_0^{(NN)}). \quad (34)$$

As discussed in Ref. [18], we separate the LECs  $L_{1A}$ ,  $L_{2A}$ , and  $L_1$  into two parts: the one consists of the effective range terms so as to reproduce the result from the effective range theory, and the other is the unfixed constants  $l_{1A}$ ,  $l_{2A}$ , and  $l_1$  which may correspond to the small correction from a mechanism in high energy such as meson exchange currents. We note that LECs do not appear for the isoscalar vector parts in Eqs. (30) and (31) due to conserved vector current (CVC). In addition, the sign for  $l_{1A}$  above is opposite to that in Refs. [21, 38].

$\Gamma_{4(1,2)}^{(NN)}(p, q)$  are four-point vertex functions for the  $NN = np, nn, pp$  channels,  $\Gamma_{3(0)}^{(NN)}(p)$  and  $\Gamma_{3(1,2)}^{(NN)}(p, q)$  are three-point vertex functions, and  $D_s^{(NN)}(p)$  and  $D_t^{(np)}(p)$  are dressed

two-nucleon propagators for spin singlet and spin triplet channels, respectively. For the  $np$  and  $nn$  channels we have

$$\Gamma_{4(1)}^{(np,nn)}(p, q) = \frac{1}{2pq} \ln \left( \frac{\gamma^2 + (p + \frac{1}{2}q)^2}{\gamma^2 + (p - \frac{1}{2}q)^2} \right), \quad (35)$$

$$\Gamma_{4(2)}^{(np,nn)}(p, q) = \frac{1}{pq} \left[ 1 - \frac{\gamma^2 + p^2 + \frac{1}{4}q^2}{2pq} \ln \left( \frac{\gamma^2 + (p + \frac{1}{2}q)^2}{\gamma^2 + (p - \frac{1}{2}q)^2} \right) \right], \quad (36)$$

$$\Gamma_{3(1)}^{(np,nn)}(p, q) = \frac{1}{q} \left[ \frac{\pi}{2} - \arcsin \left( \frac{\gamma^2 + p^2 - \frac{1}{4}q^2}{\sqrt{(\gamma^2 + p^2 + \frac{1}{4}q^2)^2 - (pq)^2}} \right) + \frac{i}{2} \ln \left( \frac{\gamma^2 + (p + \frac{1}{2}q)^2}{\gamma^2 + (p - \frac{1}{2}q)^2} \right) \right], \quad (37)$$

$$\Gamma_{3(2)}^{(np,nn)}(p, q) = -\frac{\gamma^2 + p^2 + \frac{1}{4}q^2}{q^3} \left[ \frac{\pi}{2} - \arcsin \left( \frac{\gamma^2 + p^2 - \frac{1}{4}q^2}{\sqrt{(\gamma^2 + p^2 + \frac{1}{4}q^2)^2 - (pq)^2}} \right) + \frac{i}{2} \ln \left( \frac{\gamma^2 + (p + \frac{1}{2}q)^2}{\gamma^2 + (p - \frac{1}{2}q)^2} \right) \right] + \frac{1}{q^2}(\gamma + ip), \quad (38)$$

$$D_s^{(np,nn)}(p) = \frac{1}{-\frac{1}{a_0^{(np,nn)}} + \frac{1}{2}r_0^{(np,nn)}p^2 - ip}, \quad (39)$$

$$D_t^{(np)}(p) = \frac{1}{-\gamma + \frac{1}{2}\rho_d(\gamma^2 + p^2) - ip}, \quad \Gamma_{3(0)}^{(np,nn)}(p) = 1, \quad (40)$$

where  $a_0^{(NN)}$  are scattering lengths of the  $NN$  scattering in the  $^1S_0$  channel.

For the  $pp$  channel, we include the contribution from the non-perturbative Coulomb interaction in the amplitudes; we follow the calculation method suggested by Ryberg *et al.* [39], in which Coulomb Green's functions are represented in the coordinate space satisfying ap-

propriate boundary conditions.<sup>2</sup> Thus we have

$$\Gamma_{4(1)}^{(pp)}(p, q) = \frac{e^{i\sigma_0}}{p} \int_0^\infty dr F_0(\eta, pr) j_0\left(\frac{1}{2}qr\right) e^{-\gamma r}, \quad (41)$$

$$\Gamma_{4(2)}^{(pp)}(p, q) = -e^{i\sigma_0} \frac{q}{p^2} \left[ \frac{1}{2} \int_0^\infty dr F_0(\eta, pr) j_0\left(\frac{1}{2}qr\right) e^{-\gamma r} - \frac{1}{q} \int_0^\infty dr F_0(\eta, pr) j_1\left(\frac{1}{2}qr\right) \left(\frac{1}{r} + \gamma\right) e^{-\gamma r} \right], \quad (42)$$

$$\Gamma_{3(1)}^{(pp)}(p, q) = C_\eta \int_0^\infty dr H_0^+(\eta, pr) j_0\left(\frac{1}{2}qr\right) e^{-\gamma r}, \quad (43)$$

$$\Gamma_{3(2)}^{(pp)}(p, q) = -C_\eta \left[ \frac{1}{2} \int_0^\infty dr H_0^+(\eta, pr) j_0\left(\frac{1}{2}qr\right) e^{-\gamma r} - \frac{1}{q} \int_0^\infty dr H_0^+(\eta, pr) j_1\left(\frac{1}{2}qr\right) \left(\frac{1}{r} + \gamma\right) e^{-\gamma r} \right], \quad (44)$$

$$D_s^{(pp)}(p) = \frac{1}{-\frac{1}{a_0^{(pp)}} + \frac{1}{2}r_0^{(pp)}p^2 + 2\kappa H(\eta)}, \quad \Gamma_{3(0)}^{(pp)}(p) = e^{i\sigma_0} C_\eta, \quad (45)$$

$$H(\eta) = \psi(i\eta) + \frac{1}{2i\eta} - \ln(i\eta), \quad C_\eta = \sqrt{\frac{2\pi\eta}{e^{2\pi\eta} - 1}}, \quad e^{i\sigma_0} = \sqrt{\frac{\Gamma(1+i\eta)}{\Gamma(1-i\eta)}}, \quad (46)$$

where  $H_l^+(\eta, \rho) = G_l(\eta, \rho) + iF_l(\eta, \rho)$ ;  $F_l(\eta, \rho)$  and  $G_l(\eta, \rho)$  are regular and irregular Coulomb wave functions, respectively, and  $j_l(x)$  are the spherical Bessel functions.  $\psi(z)$  is the digamma function with  $\eta = \kappa/p$ ;  $\kappa = \alpha_E m_p/2$  where  $\alpha_E$  is the fine structure constant. The  $r$ -space integrations above can be carried out analytically. The derivation and expression of those integrals are presented in Appendix A.

In a similar manner we write the amplitudes in the P-wave states as

$$\mathcal{A}_V^{3P0} = v \cdot \epsilon_{(l)} \hat{q} \cdot \vec{\epsilon}_{(d)} X_V^{3P0}, \quad (47)$$

$$\mathcal{A}_A^{3P0} = i\hat{q} \cdot (\vec{\epsilon}_{(l)} \times \vec{\epsilon}_{(d)}) X_A^{3P0}, \quad (48)$$

$$\mathcal{A}_V^{3P1} = iv \cdot \epsilon_{(l)} \vec{\epsilon}^* \cdot (\hat{q} \times \vec{\epsilon}_{(d)}) X_V^{3P1}, \quad (49)$$

$$\mathcal{A}_A^{3P1} = (\vec{\epsilon}^* \cdot \vec{\epsilon}_{(l)} \hat{q} \cdot \vec{\epsilon}_{(d)} - \vec{\epsilon}^* \cdot \vec{\epsilon}_{(d)} \hat{q} \cdot \vec{\epsilon}_{(l)}) X_A^{3P1}, \quad (50)$$

$$\mathcal{A}_V^{3P2} = v \cdot \epsilon_{(l)} \epsilon^{ij*} \hat{q}^i \epsilon_{(d)}^j X_V^{3P2}, \quad (51)$$

$$\mathcal{A}_A^{3P2} = i\epsilon^{ij*} \hat{q}^i \epsilon^{jkl} \epsilon_{(l)}^k \epsilon_{(d)}^l X_A^{3P2}, \quad (52)$$

<sup>2</sup> Recently, this method is applied to a calculation of the  $S_{E1}$  factor of the  $^{12}\text{C}(\alpha, \gamma)^{16}\text{O}$  reaction in an EFT [40].

with

$$X_V^{3P0} = -2\sqrt{\frac{2\pi\gamma}{1-\gamma\rho_d}}\Gamma_{4(3)}^{(NN)}(p, q), \quad (53)$$

$$X_V^{3P1} = \sqrt{\frac{3}{2}}X_V^{3P0}, \quad X_V^{3P2} = \sqrt{3}X_V^{3P0}, \quad (54)$$

$$X_A^{3PJ} = -g_A X_V^{3PJ}, \quad (55)$$

where  $J = 0, 1, 2$ , and  $\epsilon_i^*$  and  $\epsilon_{ij}^*$  are a vector and a symmetric tensor representing the final two nucleon for  $J = 1$  and 2 states, respectively. For the  $np$  and  $nn$  channels,  $\Gamma_{4(3)}^{(np,nn)}(p, q) = \Gamma_{4(2)}^{(np,nn)}(p, q)$ , and for the  $pp$  channel we have

$$\Gamma_{4(3)}^{(pp)}(p, q) = -\frac{e^{i\sigma_1}}{p} \int_0^\infty dr F_1(\eta, pr) j_1\left(\frac{1}{2}qr\right) e^{-\gamma r}, \quad (56)$$

with

$$e^{i\sigma_1} = \sqrt{\frac{\Gamma(2+i\eta)}{\Gamma(2-i\eta)}}. \quad (57)$$

An analytic expression of the vertex function  $\Gamma_{4(3)}^{(pp)}(p, q)$  is presented in Appendix A as well.

Summing over spins in the initial and final states, we obtain the result

$$\begin{aligned}
\sum_{\text{spins}} |A_{qq}|^2 &= 8G_F'^2 V_{ud}^2 \left\{ (3E'E - \vec{k}' \cdot \vec{k}) |X_A^{1S0}|^2 - (E'\hat{q} \cdot \vec{k} + E\hat{q} \cdot \vec{k}') \left[ X_A^{1S0*} \tilde{X}_A^{1S0} + \tilde{X}_A^{1S0*} X_A^{1S0} \right] \right. \\
&\mp 2 \left( E'\hat{q} \cdot \vec{k} - E\hat{q} \cdot \vec{k}' \right) \left[ X_A^{1S0*} \tilde{X}_V^{1S0} + \tilde{X}_V^{1S0*} X_A^{1S0} \right] \\
&+ (E'E + \vec{k}' \cdot \vec{k}) \left| \tilde{X}_A^{1S0} \right|^2 + 2(E'E - \hat{q} \cdot \vec{k}' \hat{q} \cdot \vec{k}) \left| \tilde{X}_V^{1S0} \right|^2 \\
&+ (E'E + \vec{k}' \cdot \vec{k}) \left[ |X_V^{3P0}|^2 + 2 |X_V^{3P1}|^2 + \frac{5}{3} |X_V^{3P2}|^2 \right] \\
&+ 2(E'E - \hat{q} \cdot \vec{k}' \hat{q} \cdot \vec{k}) |X_A^{3P0}|^2 + 2(2E'E - 2\vec{k}' \cdot \vec{k} - \hat{q} \cdot \vec{k}' \hat{q} \cdot \vec{k}) |X_A^{3P1}|^2 \\
&\left. + 4(20E'E - 6\vec{k}' \cdot \vec{k} + 2\hat{q} \cdot \vec{k}' \hat{q} \cdot \vec{k}) |X_A^{3P2}|^2 \right\}, \tag{58}
\end{aligned}$$

$$\begin{aligned}
\sum_{\text{spins}} |A_{np}|^2 &= 4G_F'^2 \left\{ (3E'E - \vec{k}' \cdot \vec{k}) |X_A^{1S0}|^2 - (E'\hat{q} \cdot \vec{k} + E\hat{q} \cdot \vec{k}') \left[ X_A^{1S0*} \tilde{X}_A^{1S0} + \tilde{X}_A^{1S0*} X_A^{1S0} \right] \right. \\
&\mp 2 \left( E'\hat{q} \cdot \vec{k} - E\hat{q} \cdot \vec{k}' \right) (1 - 2 \sin^2 \theta_W) \left[ X_A^{1S0*} \tilde{X}_V^{1S0} + \tilde{X}_V^{1S0*} X_A^{1S0} \right] + (E'E + \vec{k}' \cdot \vec{k}) \left| \tilde{X}_A^{1S0} \right|^2 \\
&+ 2(E'E - \hat{q} \cdot \vec{k}' \hat{q} \cdot \vec{k}) (1 - 2 \sin^2 \theta_W)^2 \left| \tilde{X}_V^{1S0} \right|^2 + 12 \sin^4 \theta_W (E'E + \vec{k}' \cdot \vec{k}) |X_{VS}^{3S1}|^2 \\
&- 12 \sin^4 \theta_W (E'\hat{q} \cdot \vec{k} + E\hat{q} \cdot \vec{k}') \left[ X_{VS}^{3S1*} \tilde{X}_{VS}^{3S1} + \tilde{X}_{VS}^{3S1*} X_{VS}^{3S1} \right] \\
&+ 12 \sin^4 \theta_W (E'E - \vec{k}' \cdot \vec{k} - 2\hat{q} \cdot \vec{k}' \hat{q} \cdot \vec{k}) \left| \tilde{X}_{VS}^{3S1} \right|^2 \\
&+ (E'E + \vec{k}' \cdot \vec{k}) (1 - 2 \sin^2 \theta_W)^2 \left[ |X_V^{3P0}|^2 + 2 |X_V^{3P1}|^2 + \frac{5}{3} |X_V^{3P2}|^2 \right] \\
&+ 2(E'E - \hat{q} \cdot \vec{k}' \hat{q} \cdot \vec{k}) |X_A^{3P0}|^2 + 2(2E'E - 2\vec{k}' \cdot \vec{k} - \hat{q} \cdot \vec{k}' \hat{q} \cdot \vec{k}) |X_A^{3P1}|^2 \\
&\left. + 4(20E'E - 6\vec{k}' \cdot \vec{k} + 2\hat{q} \cdot \vec{k}' \hat{q} \cdot \vec{k}) |X_A^{3P2}|^2 \right\}, \tag{59}
\end{aligned}$$

where we have used the spin summation relations presented in Appendix B.

### III. NUMERICAL RESULTS

First we specify the values of LECs. Low-energy constant  $l_1$  is fitted to the total cross section of the radiative neutron-proton capture process at threshold [18]. In the work of proton-proton fusion [21],  $l_{1A}$  is determined from the  $\beta$ -decay of tritium, which gives  $l_{1A} = 0.50 \pm 0.03$ . Another way to fix  $l_{1A}$  is proposed in work of neutron-neutron fusion [38], where  $l_{1A} = 0.33 \pm 0.03$ . Since a robust way to fix the value of  $l_{1A}$  is absent at present,  $l_{1A}$  is a source of uncertainty in the theoretical prediction. Without any priority to a specific value, we use both values  $l_{1A} = 0.33$  and  $0.50$  in the calculation of the total cross sections. Lagrangian term proportional to LEC  $l_{2A}$  has a derivative one order higher than the terms

| $E_\nu$ | $\nu np$ | $\bar{\nu} np$ | $e^+ nn$ | $e^- pp$ |
|---------|----------|----------------|----------|----------|
| 2       | 0        | 0              | 0        | 0.003665 |
| 3       | 0.003366 | 0.003330       | 0        | 0.04706  |
| 4       | 0.03070  | 0.03021        | 0        | 0.1567   |
| 5       | 0.09495  | 0.09291        | 0.02841  | 0.3459   |
| 6       | 0.2017   | 0.1962         | 0.1192   | 0.6230   |
| 7       | 0.3540   | 0.3425         | 0.2823   | 0.9936   |
| 8       | 0.5540   | 0.5329         | 0.5225   | 1.462    |
| 9       | 0.8029   | 0.7679         | 0.8422   | 2.032    |
| 10      | 1.102    | 1.048          | 1.242    | 2.705    |
| 11      | 1.452    | 1.373          | 1.722    | 3.485    |
| 12      | 1.853    | 1.742          | 2.282    | 4.374    |
| 13      | 2.307    | 2.157          | 2.922    | 5.374    |
| 14      | 2.813    | 2.616          | 3.640    | 6.488    |
| 15      | 3.373    | 3.119          | 4.436    | 7.716    |
| 16      | 3.987    | 3.667          | 5.309    | 9.062    |
| 17      | 4.656    | 4.259          | 6.259    | 10.53    |
| 18      | 5.380    | 4.895          | 7.285    | 12.12    |
| 19      | 6.161    | 5.576          | 8.386    | 13.83    |
| 20      | 6.998    | 6.301          | 9.563    | 15.67    |

TABLE I: Total cross section of the neutrino-deuteron scattering as functions of the incident neutrino energy. Reaction types are denoted by the particles in the final states. Incident neutrino energy  $E_\nu$  is in MeV, and the total cross sections are in units of  $10^{-42}\text{cm}^2$ .

proportional to  $l_1$  and  $l_{1A}$ . Since the perturbative expansion is performed with respect to either energy or momentum of the particles, higher order derivatives will be suppressed compared to the lower order ones. In addition, since experimental data that can constrain  $l_{2A}$  is not available, we assume  $l_{2A} = 0$  for simplicity.<sup>3</sup> Scattering lengths  $a_0^{(NN)}$  are taking

<sup>3</sup> A model calculation including meson exchange currents suggests that the  $A_0$  contribution is tiny. See Table III in Ref. [14].

the values  $-27.73$  fm,  $-18.50$  fm and  $-7.82$  fm for  $np$ ,  $nn$  and  $pp$  states, respectively, and effective ranges  $r_0^{(NN)}$  are 2.73 fm, 2.83 fm and 2.78 fm in the order of  $np$ ,  $nn$  and  $pp$  states.

Table I shows the total cross sections in units of  $10^{-42}$  cm<sup>2</sup>. For the  $np$  and  $pp$  final states, results with  $l_{1A} = 0.50$  are presented, and the results for the  $nn$  state are with  $l_{1A} = 0.33$ . General trend is monotonic increase with energy, and the rate is larger in charged-current processes than the neutral ones. For a better overall view, results in Tab. I are plotted in Fig. 2. As a benchmark for comparison with other theories, we include the result of Ref. [14], which is labeled SNPA meaning standard nuclear physics approach. In the SNPA, initial- and final-state wave functions are the solutions of Schrödinger equations with modern phenomenological  $NN$  potentials, and transition operators consist of one-body impulse approximation and two-body meson-exchange currents. In our work we use partial wave expansion of the final state up to P-wave, but the SNPA results includes states up to  $J = 6$ . Despite the huge differences in the basic formalism of the two theories in one hand, and partial waves in the final state in the other hand, predictions of the two works agree remarkably well. Recent EFT works [33, 34] show agreement to SNPA within the order of 1%. Refined comparison is in due next order.

In Tab. II, we show the difference between our work and SNPA. For each reaction channel, we calculate the differences with both  $l_{1A} = 0.33$  and 0.50. From the result of the difference, one can deduce that the total cross is larger with  $l_{1A} = 0.50$  than with 0.33 in all the reactions and energies.  $l_{1A} = 0.50$  is adopted from the work of  $pp$  fusion, and it gives better agreement to SNPA than  $l_{1A} = 0.33$  for the  $e^-pp$  reaction channel. On the other hand, total cross section of the  $e^+nn$  channel is close to SNPA with  $l_{1A} = 0.33$  than 0.50. It turns out that  $l_{1A} = 0.50$  gives better agreement to SNPA than 0.33 for the neutral-current processes. Gap between the differences of  $l_{1A} = 0.33$  and 0.50 is in the interval 0.7~1.1%, and it is weakly dependent on the reaction type and energy. We take this as a theoretical uncertainty in this work originating from the LEC  $l_{1A}$ . There are other sources of uncertainties such as truncation at NLO in the perturbative expansion and P-wave approximation in the partial wave expansion. Discussions on these uncertainties will be presented in the following paragraphs.

The relative contribution of LO amplitudes to the total cross section is shown in the column of ‘LO/total’ for the  $\nu np$  and  $e^-pp$  reactions in Table III. At energies close to threshold, LO takes 98~99% of the total. Its portion decreases monotonically as energy increases, and it reaches 91 ~ 95% at 20 MeV. This result satisfies the general behavior

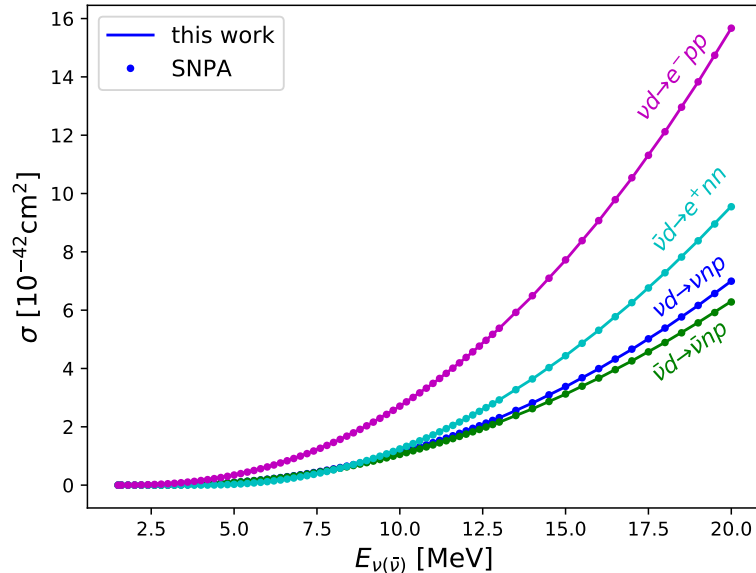


FIG. 5: Color online. Total cross sections ( $\text{cm}^2$ ) as functions of the incident neutrino energy  $E_\nu$ . Solid lines denote the result of this work for  $\nu np$  (blue),  $\bar{\nu} np$  (green),  $e^+ nn$  (cyan) and  $e^- pp$  (magenta). Dots present the result of SNPA [14].

of perturbation theory: i) lower orders dominate at low energies, ii) contribution of higher orders increase as the energy increases, iii) higher order contributions should be sufficiently smaller than those of lower orders in the considered energy range.

In order to check the validity of partial wave approximation in the final state, we consider the contribution of S-wave states. The column of ‘S-wave/total’ in Tab. III shows the ratio of cross section from S-wave contribution divided by the full contribution. In the solar neutrino energy region, the total result is absolutely dominated by the S waves. However, though it is small, contribution of higher partial waves increases with energies. In our result the contribution of P waves at  $E_\nu = 5$  MeV is 0.03% at most, and it increases to 2~3% at  $E_\nu = 20$  MeV. In the work of SNPA [14], the authors performed similar analysis of S-wave contribution. At  $E_\nu = 20$  MeV, the proportions of  $^1S_0$  state to the net value are obtained as 0.972 and 0.964 for  $\nu np$  and  $e^- pp$  reactions, respectively. These values are smaller than our results only by 0.004 and 0.008, so the two very different models give consistent predictions about the role of S-wave states in the final state. P-wave contribution is also calculated separately in [14]. At  $E_\nu = 20$  MeV, sum of S- and P-wave contribution is 99.9% of the



| $E_\nu$  | $\nu np$ |       | $\bar{\nu} np$ |       | $e^+ nn$ |      | $e^- pp$ |       |
|----------|----------|-------|----------------|-------|----------|------|----------|-------|
| $l_{1A}$ | 0.33     | 0.50  | 0.33           | 0.50  | 0.33     | 0.50 | 0.33     | 0.50  |
| 2        | -        | -     | -              | -     | -        | -    | -0.77    | -0.13 |
| 3        | -1.79    | -1.06 | -1.81          | -1.07 | -        | -    | -0.82    | -0.12 |
| 4        | -1.69    | -0.94 | -1.69          | -0.92 | -        | -    | -0.88    | -0.13 |
| 5        | -1.60    | -0.78 | -1.61          | -0.78 | 0.46     | 0.92 | -0.89    | -0.11 |
| 6        | -1.53    | -0.69 | -1.54          | -0.71 | 0.18     | 1.01 | -0.90    | -0.10 |
| 7        | -1.47    | -0.62 | -1.78          | -0.61 | 0.10     | 0.92 | -0.92    | -0.10 |
| 8        | -1.44    | -0.56 | -1.44          | -0.54 | 0.10     | 0.96 | -0.97    | -0.13 |
| 9        | -1.40    | -0.51 | -1.40          | -0.51 | 0.07     | 0.94 | -0.96    | -0.12 |
| 10       | -1.37    | -0.47 | -1.42          | -0.48 | 0.01     | 0.90 | -0.96    | -0.10 |
| 11       | -1.36    | -0.44 | -1.33          | -0.38 | 0.02     | 0.93 | -0.98    | -0.11 |
| 12       | -1.31    | -0.38 | -1.28          | -0.31 | 0.02     | 0.95 | -0.99    | -0.11 |
| 13       | -1.26    | -0.32 | -1.26          | -0.28 | -0.00    | 0.94 | -1.00    | -0.11 |
| 14       | -1.26    | -0.31 | -1.22          | -0.23 | -0.02    | 0.94 | -1.01    | -0.11 |
| 15       | -1.22    | -0.26 | -1.18          | -0.18 | -0.02    | 0.95 | -1.01    | -0.10 |
| 16       | -1.16    | -0.20 | -1.12          | -0.11 | -0.01    | 0.97 | -1.01    | -0.10 |
| 17       | -1.12    | -0.15 | -1.04          | -0.02 | 0.02     | 1.01 | -1.03    | -0.11 |
| 18       | -1.06    | -0.09 | -0.94          | 0.09  | 0.04     | 1.04 | -0.95    | -0.03 |
| 19       | -1.00    | -0.02 | -0.84          | 0.20  | 0.09     | 1.11 | -0.93    | -0.01 |
| 20       | -0.93    | 0.06  | -0.72          | 0.32  | 0.16     | 1.19 | -0.94    | -0.01 |

TABLE II: Difference of our result with respect to SNPA. Difference is calculated in % as (this work – other)/other $\times$ 100.

total result that includes the partial waves to  $J = 6$ . Therefore contributions from partial waves higher than the D state will not be a source of uncertainty at the order of 1% for the solar neutrino energies.

In Ref. [32], the authors investigated the same problem with a pionful EFT. In the work, final state wave functions contain only the S-wave states. In the column denoted by ‘S-wave/EFT\*’ in Tab. III, we present the ratio of S-wave contribution in our work to those

| $E_\nu$ | LO/total |          | S-wave/total |          | S-wave/EFT* |          |
|---------|----------|----------|--------------|----------|-------------|----------|
|         | $\nu np$ | $e^- pp$ | $\nu np$     | $e^- pp$ | $\nu np$    | $e^- pp$ |
| 5       | 0.9886   | 0.9777   | 0.9999       | 0.9997   | -           | -        |
| 10      | 0.9745   | 0.9525   | 0.9975       | 0.9963   | 0.994       | 0.999    |
| 15      | 0.9609   | 0.9288   | 0.9902       | 0.9875   | 0.997       | 1.003    |
| 20      | 0.9482   | 0.9070   | 0.9764       | 0.9723   | 1.000       | 1.007    |

TABLE III: Ratios of the LO contribution to the total (LO/total), S-wave contribution to the total (S-wave/total), and S-wave contribution in our work to that in EFT\* [32] (S-wave/EFT\*).

of EFT\*. The two theories agree in the range 0.994~1.007, so in practice the two theories predict equivalent results for the total cross section.

#### IV. SUMMARY

We considered the breakup of deuterons by neutrinos and antineutrinos at solar neutrino energies. We calculated the total cross section of the neutral-current reactions  $\nu d \rightarrow \nu np$ ,  $\bar{\nu} d \rightarrow \bar{\nu} np$ , and the charged-current ones  $\bar{\nu} d \rightarrow e^+ nn$ ,  $\nu d \rightarrow e^- pp$  in the framework of a pionless effective field theory with dibaryon fields up to the next-to-leading order. We include the Coulomb interaction between two protons non-perturbatively while analytic expressions of the amplitudes are obtained. We estimated the uncertainty of our theory by comparing our result to those obtained from various theories and models.

In the comparison to the work that employs phenomenological nucleon-nucleon potential models, contribution of the S-wave state in the final state agrees well with the result of [14], and it is confirmed that the truncation at P waves in the final state wave functions is a good approximation. Main source of the uncertainty is identified as a low-energy constant  $l_{1A}$  which determines the strength of axial four-nucleon contact interactions. The low-energy constant determined from available experimental data gives uncertainties about 1% or less.

We compared our results of S-wave contribution with those obtained from a pionful effective field theory in which expansion is performed up to next-to-next-to-next-to-leading order [32]. We found that the two theories predict practically identical results with the difference about 0.7% at most.

Convergence of the theory was checked by isolating the leading order contribution from the total. At low energies leading order contributes almost 100% of the total, and its portion decreases as the energy increases. For the  $\nu np$  reaction, leading order takes 95% of the total at  $E_\nu = 20$  MeV. This ratio of the S-wave contribution is similar to the ratio of next-to-next-to-leading order to leading order obtained in a pionless effective field theory [33]. This comparison demonstrates that the rate of convergence could be improved by the introduction of dibaryon fields.

Our result underestimates the result of benchmark calculation [14] by about 1%. On the other hand, another pionless effective field theory [33] gives a very similar result to [14], and a chiral perturbation theory [34] obtains results larger than [14] by about 1%. Therefore one can conclude that the uncertainty one can obtain from the state-of-the-art theories is about 2~3% in the solar neutrino energy range. Precise determination of LECs from experiment will be important to reduce the theoretical uncertainty.

### Acknowledgments

Work of SIA was supported by the Basic Science Research Programs through the National Research Foundation of Korea (2016R1D1A1B03930122 and 2019R1F1A1040362). Work of YHS was supported by the Rare Isotope Science Project of Institute for Basic Science funded by Ministry of Science, ICT and Future Planning and National Research Foundation of Korea (2013M7A1A1075764). Work of CHH was supported by the National Research Foundation of Korea (NRF) grant funded by the Korea government (MSIT) (No. 2018R1A5A1025563).

### Appendix A

An analytic expression of the four point vertex functions  $\Gamma_{4(1)}^{(pp)}(p, q)$  and  $\Gamma_{4(3)}^{(pp)}(p, q)$  are calculated by using formula [41],

$$F_l(\eta, \rho) = C_l(\eta) \rho^{l+1} e^{\mp i\rho} M(l+1 \mp i\eta, 2l+2, \pm 2i\rho), \quad (60)$$

where  $M(a, b, z)$  is the Kummer function and

$$C_l(\eta) = \frac{2^l e^{-\frac{\pi}{2}\eta} |\Gamma(l+1+i\eta)|}{(2l+1)!} = \frac{2^l}{(2+1)!} \sqrt{\frac{2\pi\eta}{e^{2\pi\eta}-1} \prod_{k=1}^l (\eta^2+k^2)}. \quad (61)$$

The expressions for the ( $\pm$  or  $\mp$ ) signs in Eq. (60) are identical because of a relation,  $M(a, b, z) = e^z M(b - a, b, -z)$ . Using another relation,

$$\int_0^\infty e^{-zt} t^{b-1} M(a, c, kt) dt = \Gamma(b) z^{-b} {}_2F_1(a, b, c; k/z), \quad (62)$$

with  $\text{Re}[b] > 0$ ,  $\text{Re}[z] > \max(\text{Re}[k], 0)$ , where  ${}_2F_1(a, b, c; z)$  is hypergeometric function. We have

$$\begin{aligned} \Gamma_{4(1)}^{(pp)}(p, q) &= \frac{e^{i\sigma_0}}{p} \int_0^\infty dr F_0(\eta, pr) j_0\left(\frac{1}{2}qr\right) e^{-\gamma r} \\ &= i \frac{e^{i\sigma_0}}{q} C_\eta \left[ \frac{1}{\gamma + i(p + \frac{1}{2}q)} {}_2F_1\left(1 - i\eta, 1, 2; \frac{2ip}{\gamma + i(p + \frac{1}{2}q)}\right) \right. \\ &\quad \left. - \frac{1}{\gamma + i(p - \frac{1}{2}q)} {}_2F_1\left(1 - i\eta, 1, 2; \frac{2ip}{\gamma + i(p - \frac{1}{2}q)}\right) \right], \end{aligned} \quad (63)$$

$$\begin{aligned} \Gamma_{4(3)}^{(pp)}(p, q) &= -\frac{e^{i\sigma_1}}{p} \int_0^\infty dr F_1(\eta, pr) j_1\left(\frac{1}{2}qr\right) e^{-\gamma r} \\ &= -\frac{1}{3} p e^{i\sigma_1} \sqrt{\frac{2\pi\eta(1 + \eta^2)}{e^{2\pi\eta} - 1}} \\ &\quad \times \left\{ \frac{2i}{q^2} \left[ \frac{1}{\gamma + i(p + \frac{1}{2}q)} {}_2F_1\left(2 - i\eta, 1, 4; \frac{2ip}{\gamma + i(p + \frac{1}{2}q)}\right) \right. \right. \\ &\quad \left. \left. - \frac{1}{\gamma + i(p - \frac{1}{2}q)} {}_2F_1\left(2 - i\eta, 1, 4; \frac{2ip}{\gamma + i(p - \frac{1}{2}q)}\right) \right] \right. \\ &\quad \left. - \frac{1}{q} \left[ \frac{1}{[\gamma + i(p + \frac{1}{2}q)]^2} {}_2F_1\left(2 - i\eta, 2, 4; \frac{2ip}{\gamma + i(p + \frac{1}{2}q)}\right) \right. \right. \\ &\quad \left. \left. + \frac{1}{[\gamma + i(p - \frac{1}{2}q)]^2} {}_2F_1\left(2 - i\eta, 2, 4; \frac{2ip}{\gamma + i(p - \frac{1}{2}q)}\right) \right] \right\}. \end{aligned} \quad (64)$$

The four point vertex  $\Gamma_{4(2)}^{(pp)}(p, q)$  can be represented by using the result for  $\Gamma_{4(1)}^{(pp)}(p, q)$  and an integration,

$$I_3 = \int_0^\infty dr F_0(\eta, pr) j_1\left(\frac{1}{2}qr\right) \left(\frac{1}{r} + \gamma\right) e^{-\gamma r}, \quad (65)$$

and we have

$$\begin{aligned} I_3 &= p C_\eta \sum_{n=1}^\infty (-1)^n \left[ \frac{1}{(2n+1)!} - \frac{1}{(2n)!} \right] \left(\frac{q}{2}\right)^{2n-1} \\ &\quad \times \left[ \frac{\gamma \Gamma(2n+1)}{(\gamma + ip)^{2n+1}} {}_2F_1\left(1 - i\eta, 2n+1, 2; \frac{2ip}{\gamma + ip}\right) \right. \\ &\quad \left. + \frac{\Gamma(2n)}{(\gamma + ip)^{2n}} {}_2F_1\left(1 - i\eta, 2n, 2; \frac{2ip}{\gamma + ip}\right) \right]. \end{aligned} \quad (66)$$

An analytic expression for the three point vertex function  $\Gamma_{3(1)}^{(pp)}(p, q)$  is obtained by using formulae,

$$H_l^\pm(\eta, \rho) = (\mp)^l e^{\frac{\pi}{2}\eta \pm i\sigma_l} W_{\mp i\eta, l + \frac{1}{2}}(\mp 2i\rho), \quad (67)$$

$$\int_0^\infty dt e^{-pt} t^{\nu-1} W_{\kappa, \mu}(at) = \frac{\Gamma(\mu + \nu + \frac{1}{2})\Gamma(\nu - \mu + \frac{1}{2})a^{\nu+\frac{1}{2}}}{\Gamma(\nu - \kappa + 1)(p + \frac{1}{2}a)^{\mu+\nu+\frac{1}{2}}} \times {}_2F_1\left(\mu + \nu + \frac{1}{2}, \mu - \kappa + \frac{1}{2}, \nu - \kappa + 1; \frac{p - \frac{1}{2}a}{p + \frac{1}{2}a}\right), \quad (68)$$

with  $\text{Re}[\nu \pm \mu] > -\frac{1}{2}$  and  $\text{Re}[p + \frac{1}{2}a] > 0$ , and we have

$$\begin{aligned} \Gamma_{3(1)}^{(pp)}(p, q) &= C_\eta \int_0^\infty dr H_0^+(\eta, pr) j_0\left(\frac{1}{2}qr\right) e^{-\gamma r} \\ &= C_\eta e^{\frac{\pi}{2}\eta + i\sigma_0} (-2ip) \sum_{n=0}^\infty \frac{(-1)^n}{(\gamma - ip)^{2n+2}} \left(\frac{q}{2}\right)^{2n} \frac{\Gamma(2n+1)}{\Gamma(2n+2+i\eta)} \\ &\quad \times {}_2F_1\left(2n+2, 1+i\eta, 2n+2+i\eta; \frac{\gamma+ip}{\gamma-ip}\right). \end{aligned} \quad (69)$$

The three point vertex function  $\Gamma_{3(2)}^{(pp)}(p, q)$  is represented by using the result of  $\Gamma_{3(1)}^{(pp)}(p, q)$  and an integral,

$$I_5 = \int_0^\infty dr H_0^+(\eta, pr) j_1\left(\frac{1}{2}qr\right) \left(\frac{1}{r} + \gamma\right) e^{-\gamma r}, \quad (70)$$

and we have

$$\begin{aligned} I_5 &= -2ipe^{\frac{\pi}{2}\eta + i\sigma_0} \sum_{n=1}^\infty (-1)^n \left[ \frac{1}{(2n+1)!} - \frac{1}{(2n)!} \right] \left(\frac{q}{2}\right)^{2n-1} \\ &\quad \times \left[ \frac{\gamma}{(\gamma-ip)^{2n-1}} \frac{\Gamma(2n+1)\Gamma(2n)}{\Gamma(2n+1+i\eta)} {}_2F_1\left(2n+1, 1+i\eta, 2n+1+i\eta; \frac{\gamma+ip}{\gamma-ip}\right) \right. \\ &\quad \left. + \frac{1}{(\gamma-ip)^{2n}} \frac{\Gamma(2n)\Gamma(2n-1)}{\Gamma(2n+i\eta)} {}_2F_1\left(2n, 1+i\eta, 2n+i\eta; \frac{\gamma+ip}{\gamma-ip}\right) \right]. \end{aligned} \quad (71)$$

## Appendix B

Using the spin summation relations,

$$\sum_{spins} \epsilon_{(d)i} \epsilon_{(d)j}^* = \delta_{ij}, \quad (72)$$

$$\sum_{spins} \epsilon_{(l)}^\alpha \epsilon_{(l)}^{*\beta} = 8 (k'^\alpha k^\beta + k'^\beta k^\alpha - g^{\alpha\beta} k' \cdot k \pm i\epsilon^{\alpha\beta\mu\nu} k'_\mu k_\nu), \quad (73)$$

where the  $\pm$  signs correspond to the initial neutrino and the antineutrino states, respectively, we have the spin summation relations for  $^1S_0$  channel as

$$\sum_{spins} |\vec{\epsilon}_{(l)} \cdot \vec{\epsilon}_{(d)}|^2 = 8 \left( 3E'E - \vec{k}' \cdot \vec{k} \right), \quad (74)$$

$$\sum_{spins} \vec{\epsilon}_{(l)}^* \cdot \vec{\epsilon}_{(d)}^* v \cdot \epsilon_{(l)} \hat{q} \cdot \vec{\epsilon}_{(d)} = -8 \left[ E' \hat{q} \cdot \vec{k} + E \hat{q} \cdot \vec{k}' \pm i \hat{q} \cdot (\vec{k}' \times \vec{k}) \right], \quad (75)$$

$$\sum_{spins} v \cdot \epsilon_{(l)}^* \hat{q} \cdot \vec{\epsilon}_{(d)}^* \vec{\epsilon}_{(l)} \cdot \vec{\epsilon}_{(d)} = -8 \left[ E' \hat{q} \cdot \vec{k} + E \hat{q} \cdot \vec{k}' \mp i \hat{q} \cdot (\vec{k}' \times \vec{k}) \right], \quad (76)$$

$$- \sum_{spins} \vec{\epsilon}_{(l)}^* \cdot \vec{\epsilon}_{(d)}^* i \hat{q} \cdot (\vec{\epsilon}_{(d)} \times \vec{\epsilon}_{(l)}) = \mp 16 \left( E' \hat{q} \cdot \vec{k} - E \hat{q} \cdot \vec{k}' \right), \quad (77)$$

$$\sum_{spins} i \hat{q} \cdot (\vec{\epsilon}_{(d)}^* \times \vec{\epsilon}_{(l)}^*) \vec{\epsilon}_{(l)} \cdot \vec{\epsilon}_{(d)} = \mp 16 \left( E' \hat{q} \cdot \vec{k} - E \hat{q} \cdot \vec{k}' \right), \quad (78)$$

$$\sum_{spins} |v \cdot \epsilon_{(l)} \hat{q} \cdot \vec{\epsilon}_{(d)}|^2 = 8 \left( E'E + \vec{k}' \cdot \vec{k} \right), \quad (79)$$

$$\sum_{spins} |\hat{q} \cdot (\vec{\epsilon}_{(d)} \times \vec{\epsilon}_{(l)})|^2 = 16 \left( E'E - \hat{q} \cdot \vec{k}' \hat{q} \cdot \vec{k} \right), \quad (80)$$

$$\sum_{spins} v \cdot \epsilon_{(l)}^* \hat{q} \cdot \vec{\epsilon}_{(d)}^* i \hat{q} \cdot (\vec{\epsilon}_{(d)} \times \vec{\epsilon}_{(l)}) = \sum_{spins} i \hat{q} \cdot (\vec{\epsilon}_{(d)}^* \times \vec{\epsilon}_{(l)}^*) v \cdot \epsilon_{(l)} \hat{q} \cdot \vec{\epsilon}_{(d)} = 0. \quad (81)$$

For  $^3S_1$  channel, we have

$$\sum_{spins} |v \cdot \epsilon_{(l)} \vec{\epsilon}^* \cdot \vec{\epsilon}_{(d)}|^2 = 24 \left( E'E + \vec{k}' \cdot \vec{k} \right), \quad (82)$$

$$\sum_{spins} v \cdot \epsilon_{(l)}^* \vec{\epsilon} \cdot \vec{\epsilon}_{(d)}^* \hat{q} \cdot \vec{\epsilon}_{(l)} \vec{\epsilon}^* \cdot \vec{\epsilon}_{(d)} = -24 \left[ E' \hat{q} \cdot \vec{k} + E \hat{q} \cdot \vec{k}' \mp i \hat{q} \cdot (\vec{k}' \times \vec{k}) \right], \quad (83)$$

$$\sum_{spins} \hat{q} \cdot \vec{\epsilon}_{(l)}^* \vec{\epsilon} \cdot \vec{\epsilon}_{(d)}^* v \cdot \epsilon_{(l)} \vec{\epsilon}^* \cdot \vec{\epsilon}_{(d)} = -24 \left[ E' \hat{q} \cdot \vec{k} + E \hat{q} \cdot \vec{k}' \pm i \hat{q} \cdot (\vec{k}' \times \vec{k}) \right], \quad (84)$$

$$\sum_{spins} |\hat{q} \cdot \vec{\epsilon}_{(l)} \vec{\epsilon}^* \cdot \vec{\epsilon}_{(d)}|^2 = 24 \left( E'E - \vec{k}' \cdot \vec{k} - 2 \hat{q} \cdot \vec{k}' \hat{q} \cdot \vec{k} \right). \quad (85)$$

For  $^3P_0$  channel, the terms at LO are the same as those for  $^1S_0$  channel.

For  $^3P_1$  channel at LO, using a spin summation relation for the polarization vector  $\epsilon_i$  for  $J = 1$  state,

$$\sum_{spins} \epsilon_i \epsilon_j^* = \delta_{ij}, \quad (86)$$

we have

$$\sum_{spins} |iv \cdot \epsilon_{(l)} \bar{\epsilon}^* \cdot (\hat{q} \times \bar{\epsilon}_{(d)})|^2 = 16 \left( E' E + \vec{k}' \cdot \vec{k} \right), \quad (87)$$

$$\sum_{spins} |\bar{\epsilon}^* \cdot \bar{\epsilon}_{(l)} \hat{q} \cdot \bar{\epsilon}_{(d)} - \bar{\epsilon}^* \cdot \bar{\epsilon}_{(d)} \hat{q} \cdot \bar{\epsilon}_{(l)}|^2 = 16 \left( 2E' E - 2\vec{k}' \cdot \vec{k} - \hat{q} \cdot \vec{k}' \hat{q} \cdot \vec{k} \right), \quad (88)$$

$$\begin{aligned} & \sum_{spins} iv \cdot \epsilon_{(l)} \bar{\epsilon}^* \cdot (\hat{q} \times \bar{\epsilon}_{(d)}) \left( \bar{\epsilon} \cdot \bar{\epsilon}_{(l)}^* \hat{q} \cdot \bar{\epsilon}_{(d)}^* - \bar{\epsilon} \cdot \bar{\epsilon}_{(d)}^* \hat{q} \cdot \bar{\epsilon}_{(l)}^* \right) \\ &= \sum_{spins} iv \cdot \epsilon_{(l)}^* \bar{\epsilon} \cdot (\hat{q} \times \bar{\epsilon}_{(d)}^*) \left( \bar{\epsilon}^* \cdot \bar{\epsilon}_{(l)} \hat{q} \cdot \bar{\epsilon}_{(d)} - \bar{\epsilon}^* \cdot \bar{\epsilon}_{(d)} \hat{q} \cdot \bar{\epsilon}_{(l)} \right) = 0. \end{aligned} \quad (89)$$

For  ${}^3P_2$  channel at LO, using the spin summation relation for the symmetric tensor  $\epsilon_{ij}$  for  $J = 2$  state,

$$\sum_{spins} \epsilon_{ij} \epsilon_{xy}^* = \frac{1}{2} \left( \delta_{ix} \delta_{jy} + \delta_{iy} \delta_{jx} - \frac{2}{3} \delta_{ij} \delta_{xy} \right), \quad (90)$$

we have

$$\sum_{spins} \left| v \cdot \epsilon_{(l)} \epsilon^{ij*} \hat{q}^i \epsilon_{(d)}^j \right|^2 = \frac{40}{3} \left( E' E + \vec{k}' \cdot \vec{k} \right), \quad (91)$$

$$\sum_{spins} \left| i \epsilon^{ij*} \hat{q}^i \epsilon^{jkl} \epsilon_{(l)}^k \epsilon_{(d)}^l \right|^2 = \frac{4}{3} \left( 20E' E - 6\vec{k}' \cdot \vec{k} + 2\hat{q} \cdot \vec{k}' \hat{q} \cdot \vec{k} \right), \quad (92)$$

$$\sum_{spins} v \cdot \epsilon_{(l)} \epsilon^{ij*} \hat{q}^i \epsilon_{(d)}^j \epsilon^{ij} \hat{q}^i \epsilon^{jkl} \epsilon_{(l)}^k \epsilon_{(d)}^{l*} = \sum_{spins} v \cdot \epsilon_{(l)}^* \epsilon^{ij} \hat{q}^i \epsilon_{(d)}^{j*} \epsilon^{ij*} \hat{q}^i \epsilon^{jkl} \epsilon_{(l)}^k \epsilon_{(d)}^l = 0. \quad (93)$$

- [1] J. F. Donogue, E. Golowich, and B. R. Holstein, *Dynamics of the Standard Model*, (2nd Ed., Cambridge University Press) (2014).
- [2] Q. R. Ahmad *et al.*, Phys. Rev. Lett. **87**, 071301 (2001).
- [3] Q. R. Ahmad *et al.*, Phys. Rev. Lett. **89**, 011301 (2002).
- [4] Q. R. Ahmad *et al.*, Phys. Rev. Lett. **89**, 011302 (2002).
- [5] B. Aharmim *et al.*, Phys. Rev. **72**, 055502 (2005).
- [6] E. Pasierb, H. S. Gurr, J. Lathrop, F. Reines, and H. W. Sobel, Phys. Rev. Lett. **43**, 96 (1979).
- [7] A. G. Vershinsky, *et al.*, JETP Lett. **53**, 513 (1991).
- [8] Y. Kozlov, *et al.*, Phys. At. Nucl. **63**, 1016 (2000).
- [9] S. Riley, *et al.*, Phys. Rev. C **59**, 1780 (1999).

- [10] J. A. Formaggio, and G. P. Zeller, *Rev. Mod. Phys.* **84**, 1307 (2012).
- [11] F. J. Kelly and H. Uberall, *Phys. Rev. Lett.* **16**, 145 (1966).
- [12] S. D. Ellis and J. N. Bahcall, *Nucl. Phys. A* **114**, 636 (1968).
- [13] N. Tatara, Y. Kohyama, and K. Kubodera, *Phys. Rev. C* **42**, 1694 (1990).
- [14] S. Nakamura, T. Sato, V. P. Gudkov, and K. Kubodera, *Phys. Rev. C* **63**, 034617 (2001),  
erratum; *Phys. Rev. C* **73**, 049904 (2006).
- [15] S. Nakamura *et al.*, *Nucl. Phys. A* **707**, 561 (2002).
- [16] D. B. Kaplan, *Nucl. Phys. B* **494**, 471 (1997).
- [17] S. R. Beane and M. J. Savage, *Nucl. Phys. A* **694**, 511 (2001).
- [18] S. Ando, and C. H. Hyun, *Phys. Rev. C* **72**, 014008 (2005).
- [19] S. Ando, R. H. Cyburt, S. W. Hong, and C. H. Hyun, *Phys. Rev. C* **74**, 025809 (2006).
- [20] S. Ando, J. W. Shin, C. H. Hyun, and S. W. Hong, *Phys. Rev. C* **76**, 064001 (2007).
- [21] S. Ando, J. W. Shin, C. H. Hyun, S. W. Hong, and K. Kubodera, *Phys. Lett B* **668**, 187  
(2008).
- [22] S.-I. Ando, and C. H. Hyun, *Phys. Rev. C* **86**, 024002 (2012).
- [23] S.-I. Ando, Y.-H. Song, C. H. Hyun, and K. Kubodera, *Phys. Rev. C* **83**, 064002 (2011).
- [24] Y.-H. Song, C. H. Hyun, S.-I. Ando, and K. Kubodera, *Few Body Syst.* **54**, 371 (2013).
- [25] Y.-H. Song, S.-I. Ando, and C. H. Hyun, *Phys. Rev. C* **96**, 014001 (2017).
- [26] C. H. Hyun, J. W. Shin, and S. Ando, *Mod. Phys. Lett. A* **24**, 827 (2009).
- [27] J. W. Shin, S. Ando, and C. H. Hyun, *Phys. Rev. C* **81**, 055501 (2010).
- [28] S.-i. Ando, C. H. Hyun, and J. W. Shin, *Nucl. Phys. A* **844**, 165 (2010).
- [29] J. W. Shin, S.-I. Ando, C. H. Hyun, and S. W. Hong, *Few Body Syst.* **54**, 359 (2013).
- [30] J. W. Shin, C. H. Hyun, S.-I. Ando, and S. W. Hong, *Phys. Rev. C* **88**, 035501 (2013).
- [31] S. Nasu, S. X. Nakamura, K. Sumiyoshi, T. Sato, F. Myhrer, and K. Kubodera, *Astrophys. J.* **801**, 78 (2015).
- [32] S. Ando, Y. H. Song, T.-S. Park, H. W. Fearing, and K. Kubodera, *Phys. Lett. B* **555**, 49  
(2003).
- [33] M. Butler, J.-W. Chen, and X. Kong, *Phys. Rev. C* **63**, 035501 (2001).
- [34] A. Baroni, and R. Schiavilla, *Phys. Rev. C* **96**, 014002 (2017).
- [35] W. J. Marciano and A. Sirlin, *Phys. Rev. Lett.* **71**, 3629 (1993).
- [36] S. Ando *et al.*, *Phys. Lett. B* **595**, 250 (2004).



- [37] M. Morita, *Beta Decay and Muon Capture*, (W. A. Benjamin Inc., 1973) p. 27.
- [38] S-i Ando, and K. Kubodera, Phys. Lett. B **633**, 253 (2006).
- [39] E. Ryberg, C. Forssen, H.-W. Hammer, and L. Platter, Phys. Rev. C **89**, 014325 (2014).
- [40] S.-I. Ando, Phys. Rev. C **100**, 015807 (2019).
- [41] F. W. J. Olver *et al.* (Ed.), *NIST Handbook of Mathematical Functions*, Cambridge University Press (2010).